

Set-theoretic Localization for Mobile Robots with Infrastructure-based Sensing

Xiao Li, Yutong Li, Anouck Girard, Ilya Kolmanovsky

Abstract—In this paper, we introduce a set-theoretic approach for mobile robot localization with infrastructure-based sensing. The proposed method computes sets that over-bound the robot body and orientation under an assumption of known noise bounds on the sensor and robot motion model. We establish theoretical properties and computational approaches for this set-theoretic localization approach and illustrate its application to an automated valet parking example in simulations and to omnidirectional robot localization problems in real-world experiments. We demonstrate that the set-theoretic localization method can perform robustly against uncertainty set initialization and sensor noises compared to the FastSLAM.

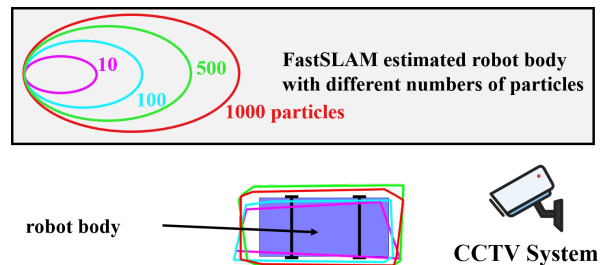


Fig. 1: FastSLAM estimated robot body.

I. INTRODUCTION

One of the major challenges for navigating mobile robots safely is in their accurate and reliable localization [1]. A promising approach is to leverage the infrastructure-based sensing and wireless communications/V2X [2]. With the advances in computing power, real-time simultaneous localization and mapping (SLAM) has become more widespread for robot localization tasks in unmapped environments [3]. In particular, with prior knowledge of the surroundings, the infrastructure-based SLAM is an appealing centralized localization approach as it reduces computational burden by treating individual agent’s localization tasks independently [4]. However, quantification of the localization uncertainties is generally handled by estimations of confidence intervals or ellipsoids within those based on probabilistic methods, e.g. Bayes filters, particle filters [1]. Explicit uncertainty bounds, which are crucial in safety-critical systems, are rarely considered in probabilistic methods.

Consider a centralized closed-circuit television (CCTV) system which collects measurements associated with the robot in Fig. 1. Suppose we use the FastSLAM to estimate the 2D robot body area. The FastSLAM is based on particle filtering. As shown in Fig. 1, localization results with fewer particles tend to underestimate the robot body. If we further use the estimated robot body in a planning module [5], an estimated area which fails to contain the entire robot body may eventually cause a collision. Though the estimated areas with 500 and 1000 particles over-bound the robot body, a larger number of particles increases sampling and computation burden and impedes online deployment. In fact, the estimated area is guaranteed to contain the robot body if and only if we sample an infinite number of particles.

The authors are with the University of Michigan, Ann Arbor, MI 48109, USA. hsaoli, yutli, anouck, ilya@umich.edu. The last author acknowledges support by the National Science Foundation under Award ECCS-1931738.

This motivates us to adopt the set-theoretic approach to perform mobile robot localization, which is inspired by [6]. Such an approach relies on the assumption of bounded uncertainties and guarantees that the nominal state is necessarily within the estimated uncertainty set. The proposed method first embeds the uncertainty bounds on estimated states and measurements into representations of intervals and convex polytopes. Then, the set-valued motion model propagation and measurements are combined to update set-valued estimates of 2D robot body area and orientation. We use the automated valet parking in which the use of infrastructure-based sensing is often assumed [7], [8], [9] as an example to validate the effectiveness of the proposed method in simulations and to compare the results with FastSLAM. We also report the results from real-world experiments which deployed an omnidirectional robot and a Lidar-based sensing system.

The main contributions of this paper are as follows: (1) We extend the theoretical results of the set-theoretic localization method to an infrastructure-based sensing setting. (2) We show that the proposed method is less sensitive to uncertainty set initialization and sensor noises compared to FastSLAM. (3) We use polytopes to approximate the uncertainty sets which reduces conservatism as compared to boxes and is still computationally efficient due to low dimensional characteristics of the problem.

II. RELATED WORK

Estimation problems [10] associated with localization in robotics have been extensively studied. Probabilistic methods such as the classical Kalman filter, particle filter, Bayesian filter, and unscented Kalman filter have been considered for the robotics localization problems [1], [10], [11]. Barrau et al. [12] design an invariant Kalman filter based on the estimation error being invariant under actions of a matrix

Lie group. For SLAM problems, new methods, for example, extended Kalman filter (EKF) SLAM [13], [14] and Fast-SLAM [15] have been developed. With the advances in computing power, matrix and graph optimization algorithms [16] such as iSAM [17] and GTSAM [18] have become feasible for implementation. SLAM algorithms which rely on visual sensors e.g. monocular, stereo, RGB-D cameras have been proposed in [19], [20], [21], [22]. With the development of machine learning, significant progress in outdoor visual place recognition and localization has been achieved [23], [24], [25], [26].

In contrast to the above probabilistic and optimization methods, set-theoretic methods enable a deterministic estimation of uncertainty bounds for robotics localization, mapping and system state estimation problems [27], [28], [29], [6], [30], [31], [32]. Inspired by [6], we propose a set-theoretic localization algorithm which use infrastructure-based sensors for mobile robots localization. We also consider applications of this algorithm to an autonomous valet parking example. We use polytopes to over-bound the uncertainty sets which is different from [6] where boxes are used and results in less conservative estimates.

III. PROBLEM FORMULATION

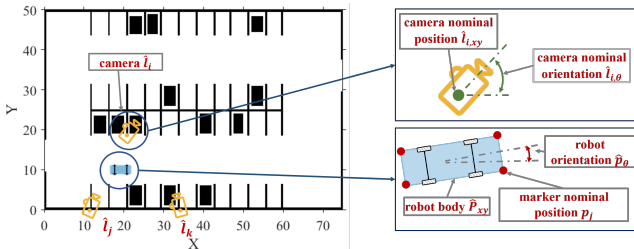


Fig. 2: Schematic diagram of an infrastructure-based localization system.

As shown in Fig. 2, suppose the localization system consists of m infrastructure-based sensors in $X - Y$ plane $\Omega \subset \mathbb{R}^2$ that are assumed to be cameras. The i^{th} camera's nominal state is $\hat{l}_i = [\hat{l}_{i,x} \ \hat{l}_{i,y} \ \hat{l}_{i,\theta}]^T$ and $i = 1, \dots, m$ where the nominal position $\hat{l}_{i,xy} = [\hat{l}_{i,x} \ \hat{l}_{i,y}]^T \in \Omega$ and the nominal orientation $\hat{l}_{i,\theta} \in [-\pi, \pi]$. A mobile robot with orientation $\hat{p}_\theta \in [-\pi, \pi]$, covered by a rectangle $\hat{P}_{xy} \subset \Omega$ of width c_w and length c_l , travels in the $X - Y$ plane. We assume that there are n detectable markers attached to the robot (in Fig. 2, $n = 4$) such that the robot body \hat{P}_{xy} is in the convex hull of the markers. We denote the i^{th} marker's nominal position by $\hat{p}_i = [\hat{p}_{i,x} \ \hat{p}_{i,y}]^T \in \Omega$. Note that in our problem setting, as long as the infrastructure-based sensor can measure the range or bearing of markers, there is no restriction on the sensor's type, i.e. it can be a monocular camera, Lidar, et al. We also note that the marker can be virtual, such as ORB [33] or SIFT [34] features with object detection [35] such as vehicle wheel detection [36], [37] to refine the region of interest.

We use the following model to represent the marker position dynamics

$$\hat{p}_i(k+1) = \hat{p}_i(k) + w(k) \quad (1)$$

where the disturbance $w(k) \in \mathbb{R}^2$ is unknown-but-bounded as $\|w(k)\|_\infty \leq \epsilon^w$ and $\epsilon^w > 0$ is a known bound. For each time step k , we are able to collect measurements $M_{i,j}(k) = \{\alpha_{i,j}(k)\}$

$$\alpha_{i,j}(k) = \text{atan2}(\hat{p}_{j,y} - \hat{l}_{i,y}, \hat{p}_{j,x} - \hat{l}_{i,x}) - \hat{l}_{i,\theta} + v_a(k)_{i,j} \quad (2)$$

where $\alpha_{i,j}(k)$ represents the angle measurement of j^{th} marker by the i^{th} camera with bounded additive noise $v_a(k)_{i,j}$ i.e. $|v_a(k)_{i,j}| \leq \epsilon^{v_a}$ where $\epsilon^{v_a} > 0$ is a known bound. Additionally, we assume each camera has a maximum detection range r_{max} such that marker satisfying $\|\hat{p}_j - \hat{l}_{i,xy}\|_2 \leq r_{max}$ is detectable by i^{th} camera.

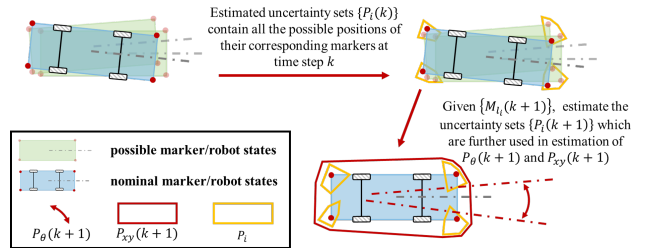


Fig. 3: Illustrations of the set-theoretic localization problem.

At previous time step k , we assume the nominal states $\{\hat{l}_i(k)\}_{i=1,\dots,m}$, $\{\hat{p}_i(k)\}_{i=1,\dots,n}$ are within the corresponding known and compact uncertainty sets $\{L_i(k)\}_{i=1,\dots,m}$, $\{P_i(k)\}_{i=1,\dots,n}$ where $L_i(k) \subset \Omega \times [-\pi, \pi]$, $P_i(k) \subset \Omega$. As shown in Fig. 3, the i^{th} uncertainty set $P_i(k)$ bounds all the possible positions of the i^{th} marker in the $X - Y$ plane such that $\hat{p}_i(k) \in P_i(k)$. Suppose we collect measurements $\{M_{i,j}(k+1)\}_{i=1,\dots,m}$ at current time step $k+1$. The goals of the set-theoretic localization method are as follows:

- 1) Propagate and update $\{L_i(k+1)\}_{i=1,\dots,m}$, $\{P_i(k+1)\}_{i=1,\dots,n}$ based on (1) and (2) such that $\hat{l}_i(k+1) \in L_i(k+1)$ for $i = 1, \dots, m$ and $\hat{p}_i(k+1) \in P_i(k+1)$ for $i = 1, \dots, n$.
- 2) Estimate two sets $P_{xy}(k+1) \subset \Omega$ and $P_\theta(k+1) \subset [-\pi, \pi]$ based on uncertainty sets $\{L_i(k+1)\}_{i=1,\dots,m}$, $\{P_i(k+1)\}_{i=1,\dots,n}$ while guarantees the robot body $\hat{P}_{xy}(k+1) \subset P_{xy}(k+1)$ and orientation $\hat{p}_\theta(k+1) \in P_\theta(k+1)$.

IV. SET-THEORETIC LOCALIZATION

In this section, we first use the robot motion model to propagate the uncertainty sets in Sec. IV-A, then update the propagated sets with measurements derived from the infrastructure-based sensors in Sec. IV-B. By incorporating the geometrical constraints between individual markers, we can improve the accuracy in estimation of the robot body and orientation in IV-C. An extension of the proposed method to the case with stereo camera-based infrastructure sensing systems is introduced in Sec. IV-D. We conclude the section with an over-approximation strategy to simplify the set operations in Sec. IV-E.

A. Motion Propagation

Based on (1) and prior to incorporating measurement information, the uncertainty sets P_i of the i^{th} marker and L_i of the i^{th} camera are updated as

$$P_i(k+1|k) = P_i(k) \oplus \mathcal{B}_\infty(\epsilon^w), \quad (3)$$

$$L_i(k+1|k) = L_i(k), \quad (4)$$

where \oplus denotes the Minkowski sum and $\mathcal{B}_\infty(\epsilon^w)$ is an ∞ -norm ball of radius ϵ^w . For camera uncertainty set propagation, to simplify the computations, we decompose L_i into two bounded sets $L_{i,xy} \subset \Omega$ and $L_{i,\theta} \subset [-\pi, \pi]$ such that $L_i \subset L_{i,xy} \times L_{i,\theta}$. This decomposition simplifies the update procedure in Sec. IV-B. This way, (4) is rewritten as

$$\begin{cases} L_{i,xy}(k+1|k) = L_{i,xy}(k), \\ L_{i,\theta}(k+1|k) = L_{i,\theta}(k). \end{cases} \quad (5)$$

B. Measurement Update

Given measurements $M_{l_i}(k+1)$ from the i^{th} camera, we first update the uncertainty set $L_{i,\theta}$, and then we sequentially update $L_{i,xy}$ and P_j . For each individual measurement $\alpha_{i,j} \in M_{l_i}(k+1)$, since $L_{i,xy}(k+1|k)$ and $P_j(k+1|k)$ are bounded, we can compute an interval bound

$$\text{atan2}(\hat{p}_{j,y} - \hat{l}_{i,y}, \hat{p}_{j,x} - \hat{l}_{i,x}) \in [\beta_{min}, \beta_{max}], \quad (6)$$

where

$$\beta_{min} = \min_{\substack{l_{i,xy} \in L_{i,xy}(k+1|k), \\ p_j \in P_j(k+1|k)}} (\text{atan2}(p_{j,y} - l_{i,y}, p_{j,x} - l_{i,x})),$$

$$\beta_{max} = \max_{\substack{l_{i,xy} \in L_{i,xy}(k+1|k), \\ p_j \in P_j(k+1|k)}} (\text{atan2}(p_{j,y} - l_{i,y}, p_{j,x} - l_{i,x})).$$

From (2) and (6), the camera nominal orientation $\hat{l}_{i,\theta} \in [\psi_{i,j}, \phi_{i,j}]$ where

$$\begin{aligned} \psi_{i,j} &= \beta_{min} - \alpha_{i,j} - \epsilon^{v_a}, \\ \phi_{i,j} &= \beta_{max} - \alpha_{i,j} + \epsilon^{v_a}. \end{aligned}$$

Given a measurement set $M_{l_i}(k+1)$, the camera nominal orientation $\hat{l}_{i,\theta}$ must be confined to the set

$$L_{i,\theta}(k+1) = L_{i,\theta}(k+1|k) \cap \left(\bigcap_{\alpha_{i,j} \in M_{l_i}} [\psi_{i,j}, \phi_{i,j}] \right). \quad (7)$$

With this updated $L_{i,\theta}(k+1)$, we are able to derive a tighter bound on $L_{i,xy}$ and P_j . We first define a set

$$\begin{aligned} L_M(p_j, \alpha_{i,j}) &:= \\ \{l \in \mathbb{R}^2 \mid |\alpha_{i,j} - \text{atan2}(-l_y, -l_x) + \theta_c| \leq \epsilon^{v_a} + \delta\theta_c\} \end{aligned} \quad (8)$$

where $\hat{l}_{i,\theta}$ is in the bounded interval $L_{i,\theta}(k+1) \subset [\theta_c - \delta\theta_c, \theta_c + \delta\theta_c]$. In the coordinate frame with p_j as the origin, the set $L_M(p_j, \alpha_{i,j})$ denotes a feasible region for l_i for which measurement $\alpha_{i,j}$ is plausible. Back to the global frame, the

i^{th} camera nominal position is in $P_j(k+1|k) \oplus L_M(p_j, \alpha_{i,j})$. Given measurements M_{l_i} , $\hat{l}_{i,xy}$ is necessarily within

$$L_{i,xy}(k+1) = L_{i,xy}(k+1|k) \cap \left(\bigcap_{\alpha_{i,j} \in M_{l_i}} (P_j(k+1|k) \oplus L_M(p_j, \alpha_{i,j})) \right). \quad (9)$$

Analogously to (8), in a reference frame centered at the i^{th} camera, the j^{th} marker position is inferred to belong to the set

$$\begin{aligned} P_M(l_i, \alpha_{i,j}) &:= \\ \{p \in \mathbb{R}^2 \mid |\alpha_{i,j} - \text{atan2}(p_y, p_x) + \theta_c| \leq \epsilon^{v_a} + \delta\theta_c\}. \end{aligned} \quad (10)$$

Considering all measurements that are corresponding to the j^{th} marker, \hat{p}_j must belong to the set,

$$P_j(k+1) = P_j(k+1|k) \cap \bigcap_{\substack{i=1, \dots, m, \\ \alpha_{i,j'} \in M_{l_i}, j'=j}} ((L_{i,xy}(k+1) \oplus P_M(l_i, \alpha_{i,j'}))) \quad (11)$$

C. Robot Body and Orientation Estimation

Before estimating the robot body and orientation, we can exploit a rigid body constraint for two arbitrary markers $\hat{p}_i, \hat{p}_j \in \{\hat{p}_i\}_{i=1, \dots, n}$ of the form $\|\hat{p}_i - \hat{p}_j\|_2 = r_{ij}$ and refine the uncertainty sets of the i^{th} and j^{th} marker positions via

$$\begin{aligned} P_i(k+1) &= P_i(k+1) \cap (P_j \oplus \mathcal{B}_2(r_{ij})), \\ P_j(k+1) &= P_j(k+1) \cap (P_i \oplus \mathcal{B}_2(r_{ij})), \end{aligned} \quad (12)$$

where $\mathcal{B}_2(r_{ij})$ represents a ℓ_2 -norm ball of radius r_{ij} .

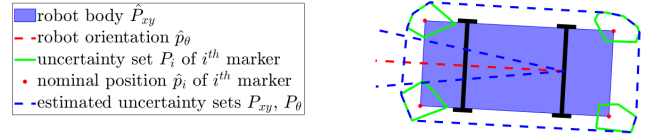


Fig. 4: Robot body estimation using convex envelope of marker uncertainty sets.

Eventually, after the set propagation by (3), (5), update via measurements by (7), (9), (11) and set refinement by rigid body constraint above, the entire robot body is over-bounded by a convex envelope $P_{xy}(k+1)$ as shown in Fig. 4 which is the convex hull of all vertices of $P_i(k+1)$, $i = 1, \dots, n$ i.e.

$$P_{xy}(k+1) := \text{convHull}(\{P_i(k+1)\}_{i=1, \dots, n}), \quad (13)$$

where $\text{convHull}()$ is the command in CORA [38], [39], [40] that calculates convex envelope of the input sets.

Meanwhile, the vector from \hat{p}_i to \hat{p}_j forms an offset angle $\Delta\theta_{ij}$ with the robot nominal orientation \hat{p}_θ . Consequently, the robot nominal orientation is within

$$P_\theta = \bigcap_{i,j=1, \dots, n, i \neq j} [\underline{\beta}_{ij} - \Delta\theta_{ij}, \bar{\beta}_{ij} - \Delta\theta_{ij}] \quad (14)$$

where $\text{atan2}(\hat{p}_{j,y} - \hat{p}_{i,y}, \hat{p}_{j,x} - \hat{p}_{i,x}) \in [\underline{\beta}_{ij}, \bar{\beta}_{ij}]$.

D. Extension to the Stereo Camera Setting

If stereo cameras are installed in place of the monocular ones, each angle measurement in (2) is coupled with a range measurement,

$$r_{i,j}(k) = \sqrt{(\hat{p}_{j,y} - \hat{l}_{i,y})^2 + (\hat{p}_{j,x} - \hat{l}_{i,x})^2} + v_r(k)_{i,j}. \quad (15)$$

where the unknown additive noise satisfies $|v_r(k)_{i,j}| \leq \epsilon^{v_r}$ and $\epsilon^{v_r} > 0$ is a known bound.

The measurement update process of $L_{i,xy}$ and P_j follows Sec. IV-B where L_M in (8) and P_M in (10) are redefined as

$$L_M(p_j, \alpha_{i,j}, r_{i,j}) := \left\{ l \in \mathbb{R}^2 \mid \begin{array}{l} |\alpha_{i,j} - \text{atan2}(-l_y, -l_x) + \theta_c| \leq \epsilon^{v_a} + \delta\theta_c \\ |r_{i,j} - \sqrt{l_x^2 + l_y^2}| \leq \epsilon^{v_r} \end{array} \right\},$$

$$P_M(l_i, \alpha_{i,j}, r_{i,j}) := \left\{ p \in \mathbb{R}^2 \mid \begin{array}{l} |\alpha_{i,j} - \text{atan2}(p_y, p_x) + \theta_c| \leq \epsilon^{v_a} + \delta\theta_c \\ |r_{i,j} - \sqrt{p_x^2 + p_y^2}| \leq \epsilon^{v_r} \end{array} \right\}.$$

The proposed method guarantees the following property (the proof is available in Appendix):

Proposition 1. Assume $\hat{l}_{i,xy}(0) \in L_{i,xy}(0)$, $\hat{l}_{i,\theta}(0) \in L_{i,\theta}(0)$, $\hat{p}_j(0) \in P_j(0)$ and $i = 1, \dots, m$, $j = 1, \dots, n$, i.e. the initial nominal states are within the initial uncertainty sets. Then, based on the set-theoretic method in (3), (5), (7), (9), (11), (12), (13) and (14), the robot body $\hat{P}_{xy}(k)$ and orientation $\hat{p}_\theta(k)$ are confined to the estimated uncertainty sets $P_{xy}(k)$, $P_\theta(k)$ for all $k > 0$, i.e. $\forall k > 0$, $\hat{P}_{xy}(k) \subset P_{xy}(k)$, $\hat{p}_\theta(k) \in P_\theta(k)$.

E. Uncertainty Set Approximation

With the problem formulation in Sec. III, the orientation and position uncertainty sets are initialized as intervals and rectangles respectively, which can be arbitrarily approximated by convex polytopes. This way, set operations in the proposed localization method can be simplified. As shown in Fig. 5, L_M in (8) and P_M in (10) can be represented by two circular sectors in the monocular camera and two annular sectors in the stereo camera. We use convex polygons to over-bound L_M and P_M where $\theta_{1,2} = (\alpha_{i,j} + \theta_c) \pm (\epsilon^{v_a} + \delta\theta_c)$ and $r_{1,2} = r_{i,j} \pm \epsilon^{v_r}$. The benefit of this over-approximation is that the set of convex polytopes is closed under Minkowski sum and intersection.

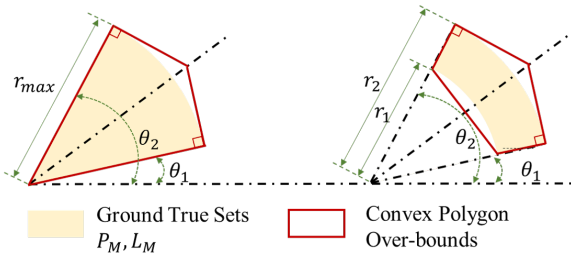


Fig. 5: Illustrations of set approximations by convex polygons.

V. SIMULATION AND EXPERIMENTAL RESULTS

In this section, we first apply the proposed set-theoretic localization method to an automated valet parking example (Fig. 6). The simulation results of the proposed method versus the FastSLAM in [15] are compared. The real-world experimental results with an omnidirectional robot and Lidar-based infrastructure sensing system are presented in Sec. V-B. The code and demonstration videos are available in [SetThmSLAM GitHub](#).

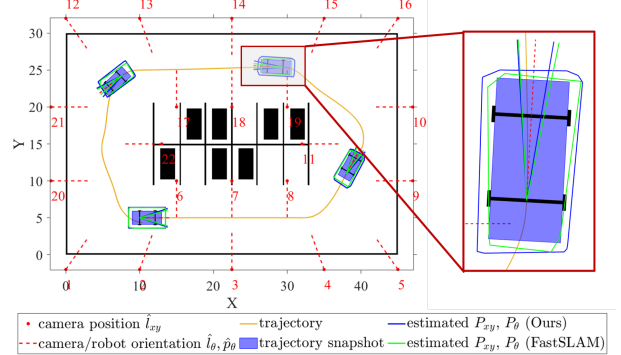


Fig. 6: Simulation results of the vehicle tracking a reference trajectory in a parking space.

A. Simulation Results

As illustrated in Fig. 6, a simulated parking space equipped with 21 cameras is built based on the Automated Parking Valet toolbox in MATLAB. Each camera has 70° field of view and 20 m measurement range. A vehicle of length $c_l = 4$ m and width $c_w = 1.8$ m is navigating within the parking space to track a reference trajectory. The proposed method is applied to localize the vehicle body and orientation and the results are compared with the ones using the FastSLAM in both monocular and stereo camera settings.

We use CORA [38], [39], [40] in MATLAB to conduct set operations between polytopes, e.g. Minkowski sum, intersections of polytopes, etc. The FastSLAM [15] is initialized with 100 particles. Each particles stores camera and marker states (i.e. $\{l_{i,xy}, l_{i,\theta}\}_{i=1,\dots,m}$, $\{p_i\}_{i=1,\dots,n}$) which are sampled from their corresponding uncertainty sets (i.e. $\{L_{i,xy}, L_{i,\theta}\}_{i=1,\dots,m}$, $\{P_i\}_{i=1,\dots,n}$). In the FastSLAM, we estimate P_{xy} using the command `enclosePoints()` in CORA to compute a convex polygon that encloses all marker positions stored in the particles. We set the disturbance bound $\epsilon^w = 2.5$ m and the sampling time $T_s = 0.5$ s.

From the snapshot in Fig. 6, the estimated uncertainty set using the FastSLAM (green solid line) sometime fails to contain the entire vehicle body. In contrast, the proposed method guarantees that the vehicle body is always contained within the estimated set (blue solid line), which validates Proposition 1.

The results using the proposed method and the FastSLAM are compared in Fig. 7 and 8. As shown in Figs. 7a-b and Figs. 8a-b, compared with the results using FastSLAM (purple line and shaded area), the volume ratio $\frac{V(P_{xy})}{c_w \cdot c_l}$ of the

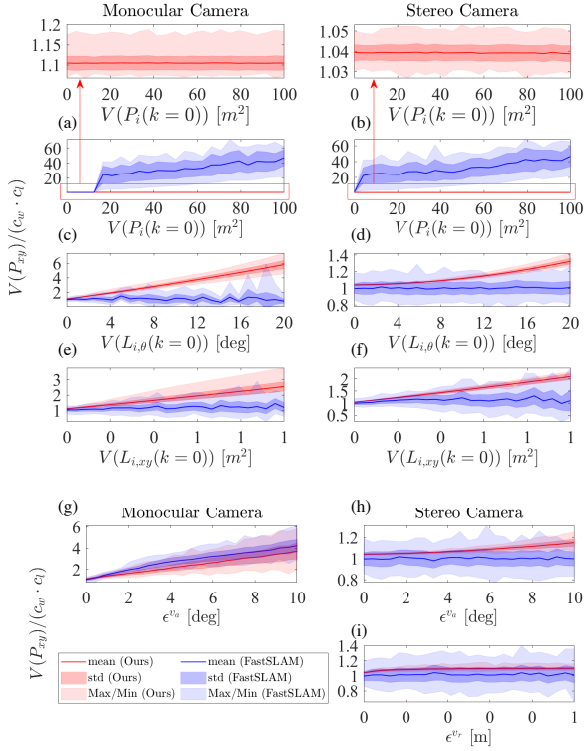


Fig. 7: Comparisons of vehicle body estimations between the proposed method and the FastSLAM in terms of the robustness against uncertainty set initialization and sensor noises.

estimated uncertainty set P_{xy} to the vehicle body does not grow with the increase of $V(P_i(k=0))$ which is the initial volume of P_i . Compared with the FastSLAM, the proposed method performs robustly against changes of $V(P_i(k=0))$. The reason is that with limited numbers of particles, higher uncertainty in the marker's initial position disadvantages the FastSLAM in estimating the probabilistic distributions of the markers' positions, thus deteriorating its performance significantly. In contrast, within the proposed method, the volume of P_{xy} largely depends on P_M through (11). P_M is computed based on the sensor noise bounds ϵ^{v_a} , ϵ^{v_r} and the estimated uncertainty bound $\delta\theta_c$ which makes the proposed method more robust against the changes of $V(P_i(k=0))$ compared to the FastSLAM.

As shown in Figs. 7c-f and Figs. 8c-f, the proposed method is more sensitive to the changes of $V(L_{i,\theta}(k=0))$ and $V(L_{i,xy}(k=0))$, which are the initial volumes of $L_{i,\theta}$ and $L_{i,xy}$, compared to the FastSLAM. It is reasonable as again in (10) and (11), the estimated uncertainty bound $\delta\theta_c$, which largely depends on $V(L_{i,\theta}(k=0))$ and $V(L_{i,xy}(k=0))$, directly affects the volume of P_{xy} and leads to degraded performance. The investigation into the method for further improving the robustness against $V(L_{i,\theta}(k=0))$ and $V(L_{i,xy}(k=0))$ is left to future work.

Finally, the comparisons of the proposed method and the FastSLAM in terms of the robustness against sensor noises

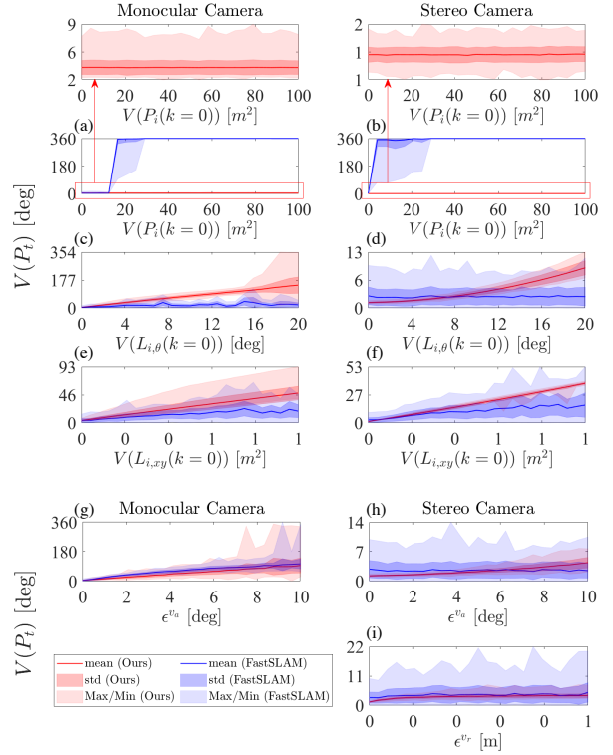


Fig. 8: Comparisons of vehicle orientation estimations between the proposed method and the FastSLAM in terms of the robustness against uncertainty set initialization and sensor noises.

are presented in Figs. 7g-i and 8g-i. Although the mean values using the proposed method and the FastSLAM are close, smaller standard deviations are achieved by deploying our proposed method. This is due to the fact that our method conducts the set estimation in a deterministic way. In contrast, at every time step in the FastSLAM, the re-sampling of particles increases the randomness of the estimated set volume, which leads to higher standard deviations.

B. Experimental Results

To further validate the proposed method, we conduct real-world experiments. We use Lidar as the infrastructure-based sensor to acquire both range and bearing measurements for the localization of an omnidirectional robot. As shown in Fig. 9, the localization system consists of three Lidars (RPLidar A1). We attach a vertical bar to the center of the robot and use it as the Lidar detection marker. Meanwhile, we attach three visual detection markers to the robot so that we can obtain the ground-true position of the robot center from the *OptiTrack* motion capture system.

We first calibrate the range and bearing measurement noise bounds as $\epsilon^{v_r} = 0.073$ m and $\epsilon^{v_a} = 8.05^\circ$, respectively. With a robot trajectory that covers the majority area of the test field, we calibrate the noise bounds as the maximum errors between measurements from *OptiTrack* and the ones from Lidars. The robot navigates in the test field with a

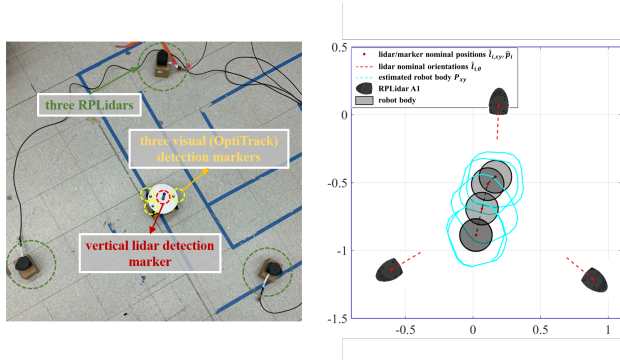


Fig. 9: Omnidirectional robot localization using lidar measurements: (Left) Photo of the test field with three RPLidars (infrastructure based sensors), and an omnidirectional robot attached with detection markers. (Right) Test results using the proposed method.

maximum speed of 0.10 m/s. As shown in Fig. 9, the proposed set theoretic localization method guarantees the estimated uncertainty set (green line) always contains the robot body (circle with a radius of 0.12 m), the test video can be found in [here](#). This result demonstrates the possibility for real-world implementation of the proposed method.

VI. CONCLUSION

In this paper, a set-theoretic localization algorithm which exploits infrastructure-based sensing has been proposed. The theoretical properties and computational approaches for this set-theoretic localization method have been established. Robustness of the proposed method to uncertainty set initialization and sensor noise has been demonstrated. Future work will focus on addressing the latency introduced by matching measurements and detected markers, and integration with downstream planning and control modules to enforce safety-related constraints.

APPENDIX

Proof of Proposition 1:

We assume the following condition

$$\hat{l}_{i,xy}(k) \in L_{i,xy}(k), \hat{l}_{i,\theta}(k) \in L_{i,\theta}(k), \hat{p}_j(k) \in P_j(k), \quad (16)$$

$$i = 1, \dots, m, j = 1, \dots, n,$$

holds for $k = 0$ during initialization. Through the propagation and update of uncertainty sets, if the condition in (16) being true for $k+1$ can be induced from same condition being satisfied at time step k , the nominal states $\hat{l}_{i,xy}$, $\hat{l}_{i,\theta}$, \hat{p}_j stay in the uncertainty sets $L_{i,xy}$, $L_{i,\theta}$, P_j respectively by principle of induction. Afterward, it's convenient to verify that the robot body and orientation are contained in P_{xy} , P_θ . For simplification, we provide the proof for the monocular camera that the stereo case resembles.

A. Motion Propagation

First, we examine the propagation process in (3), (5). Considering $\hat{p}_j(k) \in P_j(k)$ and $w(k) \in \mathcal{B}_\infty(\epsilon^w)$, the nominal state $\hat{p}_j(k+1|k) \in P_j(k+1|k)$ is guaranteed by Minkowski sum in (3). Obviously, $\hat{l}_{i,xy}(k+1|k) \in L_{i,xy}(k+1|k)$ and $\hat{l}_{i,\theta}(k+1|k) \in L_{i,\theta}(k+1|k)$ follow from (16) given (5).

B. Measurement Update

1) *Update of $L_{i,\theta}$* : By (2) and (6), $\hat{l}_{i,\theta}(k+1) \in [\psi_{i,j}, \phi_{i,j}]$ for each measurement $\alpha_{i,j}$. Indeed, considering all the measurements in M_{l_i} , the camera nominal orientation is confined to the set intersection over all possible intervals as in (7).

2) *Update of $L_{i,xy}$* : Given measurement $\alpha_{i,j}$ and in a reference frame centered at \hat{p}_j , the coordinates of the j^{th} camera $[l'_x \ l'_y]^T = \hat{l}_{i,xy}(k+1|k) - \hat{p}_j(k+1|k)$ satisfy

$$\text{atan2}(-l'_y, -l'_x) = \alpha_{i,j} + \hat{l}_{i,\theta}(k+1|k) - v_a(k+1)_{i,j}$$

by (2). Since the noise $|v_a(k+1)_{i,j}| \leq \epsilon^{v_a}$ and $\hat{l}_{i,\theta}(k+1|k) \in L_{i,\theta}(k+1|k) \subset [\theta_c - \delta\theta_c, \theta_c + \delta\theta_c]$, it can be shown that

$$\hat{l}_{i,xy}(k+1|k) - \hat{p}_j(k+1|k) \in L_M(p_j, \alpha_{i,j})$$

from (8). Given $\hat{p}_j(k+1|k) \in P_j(k+1|k)$ from propagation and equation above, the camera nominal position satisfies

$$\hat{l}_i(k+1|k) = \hat{p}_j(k+1|k) + \left(\hat{l}_{i,xy}(k+1|k) - \hat{p}_j(k+1|k) \right) \\ \in P_j(k+1|k) \oplus L_M(p_j, \alpha_{i,j}).$$

Considering all the measurements, the camera nominal position is within the set intersection over all possible $P_j(k+1|k) \oplus L_M(p_j, \alpha_{i,j})$ as in (9).

3) *Update of P_j* : It's likely that only a subset of cameras have corresponding measurements of the j^{th} marker. As above, note that

$$\hat{p}_j(k+1) - \hat{l}_{i,xy}(k+1) \in P_M(l_i, \alpha_{i,j}).$$

As $\hat{l}_{i,xy}(k+1) \in L_{i,xy}(k+1)$ from B.2, we have

$$\hat{p}_j(k+1) \in L_{i,xy}(k+1) \oplus P_M(l_i, \alpha_{i,j}).$$

Considering all M_{l_i} that contain measurement of the j^{th} marker and $\hat{p}_j(k+1) \in P_j(k+1|k)$ from A, the marker nominal position $\hat{p}_j(k+1) \in P_j(k+1)$ as derived in (11).

C. Robot Body and Orientation Estimation

Points that are at most r distance away from p_i locate in $P_i \oplus \mathcal{B}_2(r)$. If $\|\hat{p}_i - \hat{p}_j\|_2 = r_{ij}$, the marker nominal position $\hat{p}_j \in P_i \oplus \mathcal{B}_2(r_{ij})$. Thereby, the set refinement by rigid body constrains in (12) preserves the property that $\hat{p}_j \in P_j(k+1)$. Finally, given the assumption of the robot body being in the convex hull of the markers, \hat{P}_{xy} in (13) over-bounds the entire robot body P_{xy} i.e. $\hat{P}_{xy} \subset P_{xy}$. The conclusion for the robot nominal orientation that $\hat{p}_\theta \in P_\theta$ follows similarly as B.1.

REFERENCES

- [1] S. Thrun, W. Burgard, and D. Fox, *Probabilistic robotics*. MIT Press, 2005.
- [2] M. Boban, A. Kousaridas, K. Manolakis, J. Eichinger, and W. Xu, "Connected roads of the future: Use cases, requirements, and design considerations for vehicle-to-everything communications," *IEEE Vehicular Technology Magazine*, vol. 13, no. 3, pp. 110–123, 2018.
- [3] S. Thrun, "Simultaneous localization and mapping," in *Robotics and Cognitive Approaches to Spatial Mapping*. Springer, 2007, pp. 13–41.
- [4] T. Teixeira, D. Jung, and A. Savvides, "Tasking networked cctv cameras and mobile phones to identify and localize multiple people," in *Proceedings of the 12th ACM International Conference on Ubiquitous Computing*, 2010, pp. 213–222.
- [5] N. Ceccarelli, M. Di Marco, A. Garulli, and A. Giannitrapani, "A set theoretic approach to path planning for mobile robots," in *43rd IEEE Conference on Decision and Control*, vol. 1, 2004, pp. 147–152.
- [6] M. Di Marco, A. Garulli, A. Giannitrapani, and A. Vicino, "A set theoretic approach to dynamic robot localization and mapping," *Autonomous Robots*, vol. 16, no. 1, pp. 23–47, 2004.
- [7] B. Song, "Cooperative lateral vehicle control for autonomous valet parking," *International Journal of Automotive Technology*, vol. 14, no. 4, pp. 633–640, 2013.
- [8] K. Sung, J. Choi, and D. Kwak, "Vehicle control system for automatic valet parking with infrastructure sensors," in *IEEE International Conference on Consumer Electronics (ICCE)*, 2011, pp. 567–568.
- [9] M. Khalid, K. Wang, N. Aslam, Y. Cao, N. Ahmad, and M. K. Khan, "From smart parking towards autonomous valet parking: A survey, challenges and future works," *Journal of Network and Computer Applications*, p. 102935, 2020.
- [10] T. D. Barfoot, *State estimation for robotics*. Cambridge University Press, 2017.
- [11] A. Smith, *Sequential Monte Carlo methods in practice*. Springer Science & Business Media, 2013.
- [12] A. Barrau and S. Bonnabel, "Invariant kalman filtering," *Annual Review of Control, Robotics, and Autonomous Systems*, vol. 1, pp. 237–257, 2018.
- [13] P. Moutarlier and R. Chatila, "An experimental system for incremental environment modelling by an autonomous mobile robot," in *Experimental Robotics I*. Springer, 1990, pp. 327–346.
- [14] P. Moutarlier, "Stochastic multisensory data fusion for mobile robot location and environment modeling," *Proceedings of International Symposium on Robotics Research*, 1989.
- [15] M. Montemerlo, S. Thrun, D. Koller, B. Wegbreit *et al.*, "Fastslam: A factored solution to the simultaneous localization and mapping problem," *AAAI Innovative Applications of Artificial Intelligence*, vol. 593598, 2002.
- [16] G. Grisetti, R. Kümmerle, C. Stachniss, and W. Burgard, "A tutorial on graph-based slam," *IEEE Intelligent Transportation Systems Magazine*, vol. 2, no. 4, pp. 31–43, 2010.
- [17] M. Kaess, A. Ranganathan, and F. Dellaert, "isam: Incremental smoothing and mapping," *IEEE Transactions on Robotics*, vol. 24, no. 6, pp. 1365–1378, 2008.
- [18] F. Dellaert, "Factor graphs and gtsam: A hands-on introduction," Georgia Institute of Technology, Tech. Rep., 2012.
- [19] R. Mur-Artal, J. M. M. Montiel, and J. D. Tardos, "Orb-slam: a versatile and accurate monocular slam system," *IEEE Transactions on Robotics*, vol. 31, no. 5, pp. 1147–1163, 2015.
- [20] J. Engel, T. Schöps, and D. Cremers, "Lsd-slam: Large-scale direct monocular slam," in *European Conference on Computer Vision*. Springer, 2014, pp. 834–849.
- [21] A. J. Davison, I. D. Reid, N. D. Molton, and O. Stasse, "Monoslam: Real-time single camera slam," *IEEE Transactions on Pattern Analysis and Machine Intelligence*, vol. 29, no. 6, pp. 1052–1067, 2007.
- [22] T. Whelan, M. Kaess, H. Johannsson, M. Fallon, J. J. Leonard, and J. McDonald, "Real-time large-scale dense rgb-d slam with volumetric fusion," *The International Journal of Robotics Research*, vol. 34, no. 4-5, pp. 598–626, 2015.
- [23] S. Lowry, N. Sünderhauf, P. Newman, J. J. Leonard, D. Cox, P. Corke, and M. J. Milford, "Visual place recognition: A survey," *IEEE Transactions on Robotics*, vol. 32, no. 1, pp. 1–19, 2016.
- [24] T. Naseer, G. L. Oliveira, T. Brox, and W. Burgard, "Semantics-aware visual localization under challenging perceptual conditions," in *IEEE International Conference on Robotics and Automation*, 2017, pp. 2614–2620.
- [25] K. Pirker, M. Rütger, and H. Bischof, "Cd slam-continuous localization and mapping in a dynamic world," in *IEEE/RSJ International Conference on Intelligent Robots and Systems*, 2011, pp. 3990–3997.
- [26] R. Arandjelović, P. Gronat, A. Torii, T. Pajdla, and J. Sivic, "NetVLAD: CNN architecture for weakly supervised place recognition," in *IEEE Conference on Computer Vision and Pattern Recognition*, 2016.
- [27] U. D. Hanebeck and G. Schmidt, "Set theoretic localization of fast mobile robots using an angle measurement technique," in *Proceedings of IEEE International Conference on Robotics and Automation*, vol. 2, 1996, pp. 1387–1394.
- [28] T. Alamo, J. M. Bravo, and E. F. Camacho, "Guaranteed state estimation by zonotopes," *Automatica*, vol. 41, no. 6, pp. 1035–1043, 2005.
- [29] D. Merhy, C. Stoica Maniu, T. Alamo, E. F. Camacho, S. Ben Chabane, T. Chevet, M. Makarov, and I. Hinojosa, "Guaranteed set-membership state estimation of an octorotor's position for radar applications," *International Journal of Control*, vol. 93, no. 11, pp. 2760–2770, 2020.
- [30] M. Di Marco, "Set-membership estimation techniques for mobile robotics applications," Ph.D. dissertation, Bologna University, 2001.
- [31] H. Wang, I. Kolmanovsky, and J. Sun, "Zonotope-based recursive estimation of the feasible solution set for linear static systems with additive and multiplicative uncertainties," *Automatica*, vol. 95, pp. 236–245, 2018.
- [32] I. Kolmanovsky, I. Sivergina, and J. Sun, "Simultaneous input and parameter estimation with input observers and set-membership parameter bounding: Theory and an automotive application," *International Journal of Adaptive Control and Signal Processing*, vol. 20, no. 5, pp. 225–246, 2006.
- [33] E. Rublee, V. Rabaud, K. Konolige, and G. Bradski, "Orb: An efficient alternative to sift or surf," in *IEEE International Conference on Computer Vision*, 2011, pp. 2564–2571.
- [34] D. G. Lowe, "Object recognition from local scale-invariant features," in *Proceedings of the 7th IEEE International Conference on Computer Vision*, vol. 2, 1999, pp. 1150–1157.
- [35] C. Papageorgiou and T. Poggio, "A trainable system for object detection," *International Journal of Computer Vision*, vol. 38, no. 1, pp. 15–33, 2000.
- [36] O. Achler and M. M. Trivedi, "Camera based vehicle detection, tracking, and wheel baseline estimation approach," in *Proceedings of the 7th International IEEE Conference on Intelligent Transportation Systems*, 2004, pp. 743–748.
- [37] —, "Vehicle wheel detector using 2d filter banks," in *IEEE Intelligent Vehicles Symposium*, 2004, pp. 25–30.
- [38] M. Althoff, "An introduction to cora 2015," in *Proceedings of the Workshop on Applied Verification for Continuous and Hybrid Systems*, 2015.
- [39] M. Althoff and D. Grebenyuk, "Implementation of interval arithmetic in cora 2016," in *Proceedings of the 3rd International Workshop on Applied Verification for Continuous and Hybrid Systems*, 2016.
- [40] M. Althoff, D. Grebenyuk, and N. Kochdumper, "Implementation of taylor models in cora 2018," in *Proceedings of the 5th International Workshop on Applied Verification for Continuous and Hybrid Systems*, 2018.